Chapter 6

Background Estimation

The relevant Standard Model processes contributing to multilepton final states are diboson production (WZ, ZZ), production of a top quark pair in association with a weak gauge boson ($t\bar{t}+V$), and triboson production ($VVV^{(*)}$, where $V = W$ or Z). Examples tree-level Feynman diagrams of these processes are shown in figure 6.1. These backgrounds, called *prompt* backgrounds, are estimated using Monte Carlo (MC) simulation, as described in section 6.1. Significant backgrounds also arise from processes where at least one reconstructed lepton is due to the semileptonic decay of a hadron, the misidentification of a jet, or the asymmetric conversion of a photon in the detector; such backgrounds are called *reducible* backgrounds. These backgrounds are estimated using either MC simulation or a data-driven technique called the *fake factor* method, and are described in section 6.2.

6.1 Prompt Backgrounds

The prompt backgrounds are estimated using Monte Carlo simulation. The hard-scattering processes are modeled by dedicated event generators, possibly including the emission of additional partons. Additional QCD radiation is modeled using a parton shower. The detector response to the simulated events is simulated with the ATLAS simulation framework [1] using the GEANT4 toolkit [2]. Pileup is included by overlaying simulated minimum-bias interactions from PYTHIA [3] on the hard scattering event. Simulated events are assigned weights to reproduce the observed pileup distributions in data, and also to account for small differences in the trigger, reconstruction, and identification efficiencies between simulation and data.

The details of the modeling of each sample are described below. The generator, parton shower, PDF set, underlying event tune, and accuracy of theoretical cross section for samples are summarized in table 6.1.

- SHERPA [4] is used to model WW, WZ, and ZZ production. Both bosons in the events decay leptonically. Up to three additional parton emissions are included in the matrix element. An important feature of SHERPA is that it accurately models the $W + \gamma^*$

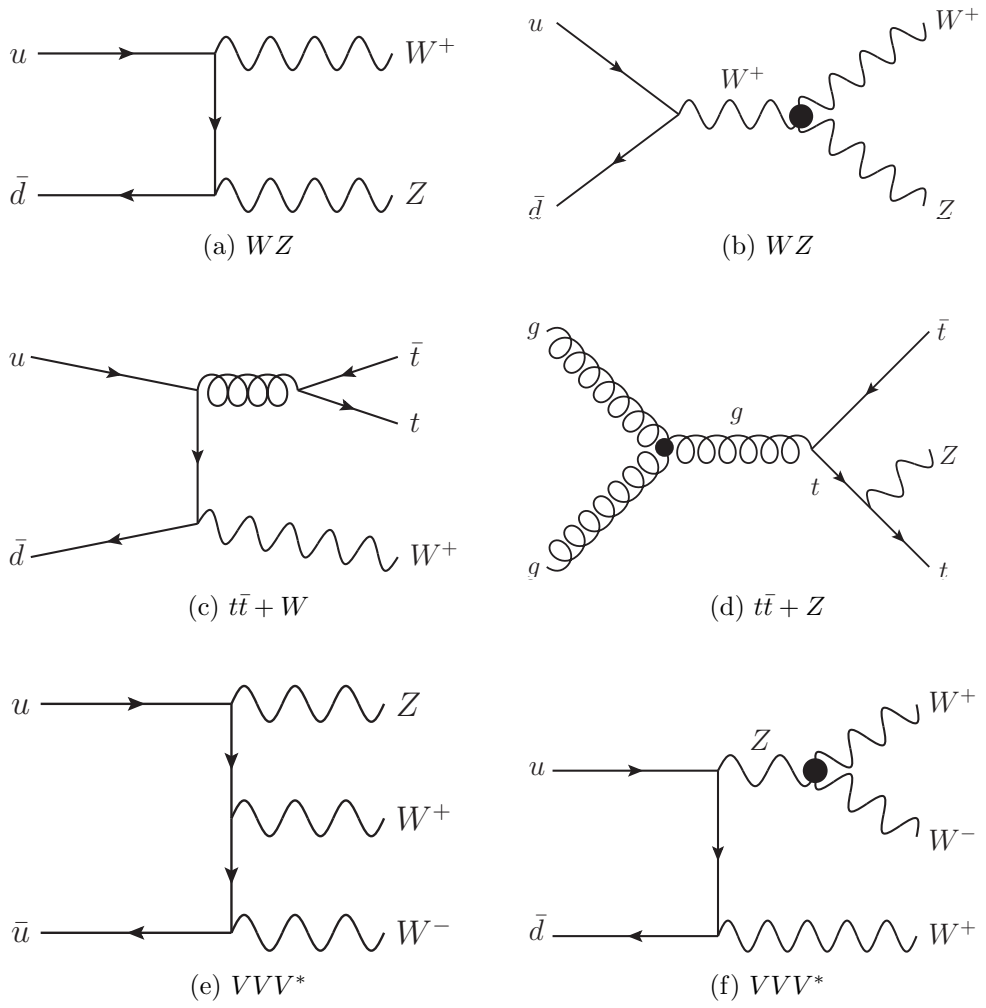

Figure 6.1: Example tree-level Feynman diagrams of Standard Model processes leading to trilepton final states.

Process	Generator	Parton shower and hadr.	PDF set	UE tune	Cross section
WZ	SHERPA 1.4.3	SHERPA	CT10 [6]	SHERPA	NLO
ZZ	SHERPA 1.4.5	SHERPA	CT10	SHERPA	NLO
$t\bar{t}+W/Z$	MADGRAPH 5.1.3.33	PYTHIA 6.426	CTEQ6L1 [7]	AUET2B [8]	NLO
$VVV^{(*)}$	MADGRAPH 5.1.3.33	PYTHIA 6.426	CTEQ6L1	AUET2B	LO
$Z+\gamma$	SHERPA	SHERPA	CT10	SHERPA	LO

Table 6.1: Summary of the primary background MC samples used in this analysis. The generator, parton shower and hadronization, PDF, underlying event tune, and the order of the cross section calculation are shown for each sample.

and $Z+\gamma^*$ contributions down to very low γ^* masses; for electron decays, a cut of $m(ee) > 100$ MeV is applied, while for muon and tau decays, SHERPA naturally cuts off the divergence. To increase the statistics in the phase space relevant for this analysis, the WZ samples requires at least two leptons to have $p_{\mathrm{T}} > 5$ GeV. Finally, the WZ sample also treats the b and c quarks as massive, which improves the modeling of heavy flavor jets at the cost of increased computation time.

- $t\bar{t}+V$ production is modeled with MADGRAPH [5], with PYTHIA for the parton shower.
- $WWW^{(*)}$, $ZWW^{(*)}$, and $ZZZ^{(*)}$ are modeled using MADGRAPH, with PYTHIA for the parton shower. Their contributions to all the signal regions are negligible.

6.2 Reducible Backgrounds

The reducible backgrounds encompass a variety of processes in which one or more reconstructed lepton arises due to a non-prompt process or a misidentification of a jet. Such leptons are referred to here as *fake*[1]. Sources of such leptons include semileptonic hadron decays, misidentified jets, particles penetrating the calorimeter and leaving hits in the muon spectrometers, and asymmetric photon conversions in the detector. The backgrounds are estimated using simulation or a data-driven technique, depending on the source. The contribution from $Z+\gamma$, where the photon converts asymmetrically and is reconstructed as an electron, is estimated using SHERPA, as shown in table 6.1. The events are reweighted to account for an observed mismodeling in the conversion rate, as described in section 10.1.1. Other reducible contributions are estimated using a data-driven technique called the *fake factor* method.

6.2.1 Fake Factor Method

The fake factor method estimates the reducible backgrounds in each signal region by characterizing the fake leptons in terms of quantities sensitive to the non-prompt or fake process,

[1]Note that real leptons from, e.g., semileptonic heavy flavor decays are included in the fake leptons.

such as isolation, impact parameter, or particle identification cuts. Two orthogonal sets of reconstructed leptons are defined: *numerator* leptons (N) satisfy the nominal signal lepton selection criteria, while *denominator* leptons (D) satisfy most of the nominal selection criteria, except with inverted requirements on quantities sensitive to the reducible process. The reducible background is estimated in a data-driven way from a control region consisting of events with a mix of numerator and denominator leptons, together with a parametrization of the relationship between numerators and denominators.

The relationship between numerator and denominator objects is called the *fake factor*, f, defined as the ratio of the number of fake leptons satisfying the numerator criteria to those satisfying the denominator criteria. The fake factor is measured in a control region enriched in fake leptons. The success of the method depends largely on the extrapolation of the f from the measurement control region to the signal regions. To capture the dependence on the event kinematics, f can be measured as a function of various lepton or event variables; in this dissertation, the fake factors are all measured in bins of lepton p_{T} and η.

Once f has been measured, the reducible background is determined as follows. In signal events with three or more leptons, any subset of the leptons could be real or fake. For example, an event might contain two real leptons from a Drell-Yan process plus a non-prompt third lepton from a semileptonic heavy flavor decay. Label such an event $\ell_1^{\mathrm{R}}\ell_2^{\mathrm{R}}\ell_3^{\mathrm{F}}$, indicating the classification of the three leptons at truth level as either real (R) or fake (F). The ordering of the letters corresponds to some canonical ordering of the leptons, such as p_{T} ordering. If an event contains one lepton from a W decay plus two non-prompt or fake leptons, the event would be labeled $\ell_1^{\mathrm{R}}\ell_2^{\mathrm{F}}\ell_3^{\mathrm{F}}$ (or $\ell_1^{\mathrm{F}}\ell_2^{\mathrm{R}}\ell_3^{\mathrm{F}}$ or $\ell_1^{\mathrm{F}}\ell_2^{\mathrm{F}}\ell_3^{\mathrm{R}}$).

The quantity we desire to determine is the number of events containing three real leptons, $n_{\ell_1^{\mathrm{R}}\ell_2^{\mathrm{R}}\ell_3^{\mathrm{R}}}$. The quantity actually measured in a signal region is the number of events containing three numerator objects, $n_{\ell_1^{\mathrm{N}}\ell_2^{\mathrm{N}}\ell_3^{\mathrm{N}}}$. Any of these numerator objects could be real or fake, so the sample can be decomposed as:

$$n_{\ell_1^{\mathrm{N}}\ell_2^{\mathrm{N}}\ell_3^{\mathrm{N}}} = n_{\ell_1^{\mathrm{R}}\ell_2^{\mathrm{R}}\ell_3^{\mathrm{R}}} + n_{\ell_1^{\mathrm{R}}\ell_2^{\mathrm{R}}\ell_3^{\mathrm{F}}} + n_{\ell_1^{\mathrm{R}}\ell_2^{\mathrm{F}}\ell_3^{\mathrm{R}}} + n_{\ell_1^{\mathrm{R}}\ell_2^{\mathrm{F}}\ell_3^{\mathrm{F}}} + \tag{6.1}$$

$$+ n_{\ell_1^{\mathrm{F}}\ell_2^{\mathrm{R}}\ell_3^{\mathrm{R}}} + n_{\ell_1^{\mathrm{F}}\ell_2^{\mathrm{R}}\ell_3^{\mathrm{F}}} + n_{\ell_1^{\mathrm{F}}\ell_2^{\mathrm{F}}\ell_3^{\mathrm{R}}} + n_{\ell_1^{\mathrm{F}}\ell_2^{\mathrm{F}}\ell_3^{\mathrm{F}}} \tag{6.2}$$

The reducible background prediction is $n_{\ell_1^{\mathrm{N}}\ell_2^{\mathrm{N}}\ell_3^{\mathrm{N}}} - n_{\ell_1^{\mathrm{R}}\ell_2^{\mathrm{R}}\ell_3^{\mathrm{R}}}$, the number of signal events where at least one lepton is fake. To determine the other terms, we use events with one or more denominator leptons. For example, consider $\ell_1^{\mathrm{D}}\ell_2^{\mathrm{N}}\ell_3^{\mathrm{N}}$ events, where the first lepton is a denominator and the remaining leptons are numerators. Assuming that the denominator lepton is always a fake lepton, the number of $\ell_1^{\mathrm{D}}\ell_2^{\mathrm{N}}\ell_3^{\mathrm{N}}$ events, each weighted by the fake factor f corresponding to the denominator lepton (represented schematically by $n_{\ell_1^{\mathrm{D}}\ell_2^{\mathrm{N}}\ell_3^{\mathrm{N}}} f_1$), equals the number of $\ell_1^{\mathrm{N}}\ell_2^{\mathrm{N}}\ell_3^{\mathrm{N}}$ events where the first lepton is fake:

$$n_{\ell_1^{\mathrm{D}}\ell_2^{\mathrm{N}}\ell_3^{\mathrm{N}}} f_1 = n_{\ell_1^{\mathrm{F}}\ell_2^{\mathrm{R}}\ell_3^{\mathrm{R}}} + n_{\ell_1^{\mathrm{F}}\ell_2^{\mathrm{R}}\ell_3^{\mathrm{F}}} + n_{\ell_1^{\mathrm{F}}\ell_2^{\mathrm{F}}\ell_3^{\mathrm{R}}} + n_{\ell_1^{\mathrm{F}}\ell_2^{\mathrm{F}}\ell_3^{\mathrm{F}}}. \tag{6.3}$$

Similarly, the remaining permutations of numerators and denominators yield:

$$n_{\ell_1^{\mathrm{N}}\ell_2^{\mathrm{D}}\ell_3^{\mathrm{N}}} f_2 = n_{\ell_1^{\mathrm{R}}\ell_2^{\mathrm{F}}\ell_3^{\mathrm{R}}} + n_{\ell_1^{\mathrm{R}}\ell_2^{\mathrm{F}}\ell_3^{\mathrm{F}}} + n_{\ell_1^{\mathrm{F}}\ell_2^{\mathrm{F}}\ell_3^{\mathrm{R}}} + n_{\ell_1^{\mathrm{F}}\ell_2^{\mathrm{F}}\ell_3^{\mathrm{F}}} \tag{6.4}$$

$$n_{\ell_1^{\mathrm{N}}\ell_2^{\mathrm{N}}\ell_3^{\mathrm{D}}} f_3 = n_{\ell_1^{\mathrm{R}}\ell_2^{\mathrm{R}}\ell_3^{\mathrm{F}}} + n_{\ell_1^{\mathrm{R}}\ell_2^{\mathrm{F}}\ell_3^{\mathrm{F}}} + n_{\ell_1^{\mathrm{F}}\ell_2^{\mathrm{R}}\ell_3^{\mathrm{F}}} + n_{\ell_1^{\mathrm{F}}\ell_2^{\mathrm{F}}\ell_3^{\mathrm{F}}} \tag{6.5}$$

$$n_{\ell_1^{\mathrm{D}}\ell_2^{\mathrm{D}}\ell_3^{\mathrm{N}}} f_1 f_2 = n_{\ell_1^{\mathrm{F}}\ell_2^{\mathrm{F}}\ell_3^{\mathrm{R}}} + n_{\ell_1^{\mathrm{F}}\ell_2^{\mathrm{F}}\ell_3^{\mathrm{F}}} \tag{6.6}$$

$$n_{\ell_1^{\mathrm{D}}\ell_2^{\mathrm{N}}\ell_3^{\mathrm{D}}} f_1 f_3 = n_{\ell_1^{\mathrm{F}}\ell_2^{\mathrm{R}}\ell_3^{\mathrm{F}}} + n_{\ell_1^{\mathrm{F}}\ell_2^{\mathrm{F}}\ell_3^{\mathrm{F}}} \tag{6.7}$$

$$n_{\ell_1^{\mathrm{N}}\ell_2^{\mathrm{D}}\ell_3^{\mathrm{D}}} f_2 f_3 = n_{\ell_1^{\mathrm{R}}\ell_2^{\mathrm{F}}\ell_3^{\mathrm{F}}} + n_{\ell_1^{\mathrm{F}}\ell_2^{\mathrm{F}}\ell_3^{\mathrm{F}}} \tag{6.8}$$

$$n_{\ell_1^{\mathrm{D}}\ell_2^{\mathrm{D}}\ell_3^{\mathrm{D}}} f_1 f_2 f_3 = n_{\ell_1^{\mathrm{F}}\ell_2^{\mathrm{F}}\ell_3^{\mathrm{F}}} \tag{6.9}$$

These equations contain eight equations and eight unknowns, so the system can be solved for the reducible background prediction:

$$\ell_1^{\mathrm{N}}\ell_2^{\mathrm{N}}\ell_3^{\mathrm{N}} - \ell_1^{\mathrm{R}}\ell_2^{\mathrm{R}}\ell_3^{\mathrm{R}} = \left(\ell_1^{\mathrm{N}}\ell_2^{\mathrm{N}}\ell_3^{\mathrm{D}} f_3 + \ell_1^{\mathrm{N}}\ell_2^{\mathrm{D}}\ell_3^{\mathrm{N}} f_2 + \ell_1^{\mathrm{D}}\ell_2^{\mathrm{N}}\ell_3^{\mathrm{N}} f_1\right) \tag{6.10}$$

$$- \left(\ell_1^{\mathrm{N}}\ell_2^{\mathrm{D}}\ell_3^{\mathrm{D}} f_2 f_3 + \ell_1^{\mathrm{D}}\ell_2^{\mathrm{N}}\ell_3^{\mathrm{D}} f_1 f_3 + \ell_1^{\mathrm{D}}\ell_2^{\mathrm{D}}\ell_3^{\mathrm{N}} f_1 f_2\right) \tag{6.11}$$

$$+ \ell_1^{\mathrm{D}}\ell_2^{\mathrm{D}}\ell_3^{\mathrm{D}} f_1 f_2 f_3 \tag{6.12}$$

Note that throughout this method, we have assumed that the leptons used for the measurement of f and the denominator leptons in trilepton events are always reducible leptons. In practice, real leptons contaminate both of these samples. The contribution from real denominator leptons is accounted for using simulation, where the lepton can be classified as real or fake using the truth record of the event.

The remainder of this chapter presents the measurement of the fake factors f for electrons, muons, and tau leptons.

6.2.2 Electron Fake Factors

The background estimation for reducible electrons targets the reducible contribution from two sources: semileptonic heavy flavor decays and misidentified light hadrons. The electron denominator objects are required to pass all of the nominal signal electron requirements except for either failing the `medium++` requirements and passing the `loose++` requirements, or having a larger transverse impact parameter, $3 < \frac{d_0}{\sigma_{d_0}} < 10$, as shown in table 6.2. The two inverted requirements are combined in an exclusive OR. The parameter space between `medium++` and `loose++`, rather than between `tight++` and `medium++`, is used for two reasons. First, for the model-independent trilepton analysis (chapter 7), electrons passing `medium++` and failing `loose++` are used to define a validation region to test the fake factor method. Second, requiring the electrons to fail `medium++` reduces the prompt contamination in the denominator sample.

Besides passing all of the remaining cuts listed in table 5.2, denominator electrons with $p_{\mathrm{T}} < 24\,\mathrm{GeV}$ must pass an additional cut designed to mitigate an observed inefficiency for loose offline electrons with respect to the loose electron triggers used in the measurement of

the fake factors. The inefficiency is likely due to the lack of Gaussian sum filter (GSF) tracking [9] at the trigger level. In order to remove electrons with large amounts of bremsstrahlung whose tracks may not be reconstructed by the non-GSF tracking algorithm in the trigger, denominator electrons are required to satisfy the `tight++` requirements on the matching between the track and the calorimeter cluster in $\Delta\eta$ and $\Delta\phi$. The cut is not applied to electrons with $p_{\mathrm{T}} > 24\,\mathrm{GeV}$, as photon triggers with no track requirement are used in this range.

Criteria	Numerator	Denominator
IsEM ID	`tight++`	!`medium++` && `loose++`
Impact Parameter Significance	$\frac{\lvert d_0\rvert}{\sigma_{d_0}} < 3$	$3 < \frac{\lvert d_0\rvert}{\sigma_{d_0}} < 10$

Table 6.2: Electron denominator definitions. The denominators are taken to be an exclusive OR combination of the two selection inversions. Additionally, denominator objects must pass the tight requirement on the $\Delta\eta$ and $\Delta\phi$ between the track and the cluster.

The fake factors are measured in a control sample of single-electron events, using the entire $20.3\,\mathrm{fb}^{-1}$ 2012 dataset. The triggers used to collect events are listed in table 6.3; photon triggers are used where available ($p_{\mathrm{T}} > 24\,\mathrm{GeV}$), and loose electron triggers are used otherwise ($15\,\mathrm{GeV} < p_{\mathrm{T}} < 24\,\mathrm{GeV}$).

p_{T} range [GeV]	Trigger Name	Average 2012 Prescale
15–17	`EF_e5_loose0`	56080.5
17–24	`EF_e15vh_loose0`	1549.7
24–45	`EF_g20_loose`	4412.6
45–65	`EF_g40_loose`	348.3
65–85	`EF_g60_loose`	80.9
85–105	`EF_g80_loose`	28.5
105–125	`EF_g100_loose`	13.0
125–210	`EF_g120_loose`	1.0
>210	`EF_g200_etcut`	1.0

Table 6.3: Triggers used to collect electron numerator and denominator objects in various p_{T} ranges, along with the average trigger prescale in 2012. Electron triggers are denoted by `EF_e`, and photon triggers by `EF_g`. The number indicates the E_{T} cut in GeV. Triggers labeled `loose` or `loose0` impose shower shape requirements similar to the offline `loose++` electron identification criteria. The trigger labeled `etcut` only imposes the E_{T} cut, with no shower shape requirement.

Events are required to have $m_{\mathrm{T}} < 40\,\mathrm{GeV}$ and $E_{\mathrm{T}}^{\mathrm{miss}} < 40\,\mathrm{GeV}$ to suppress contamination from single-W production, where m_{T} is the transverse mass of the electron and missing transverse energy in the event. The events are also required to have exactly one electron,

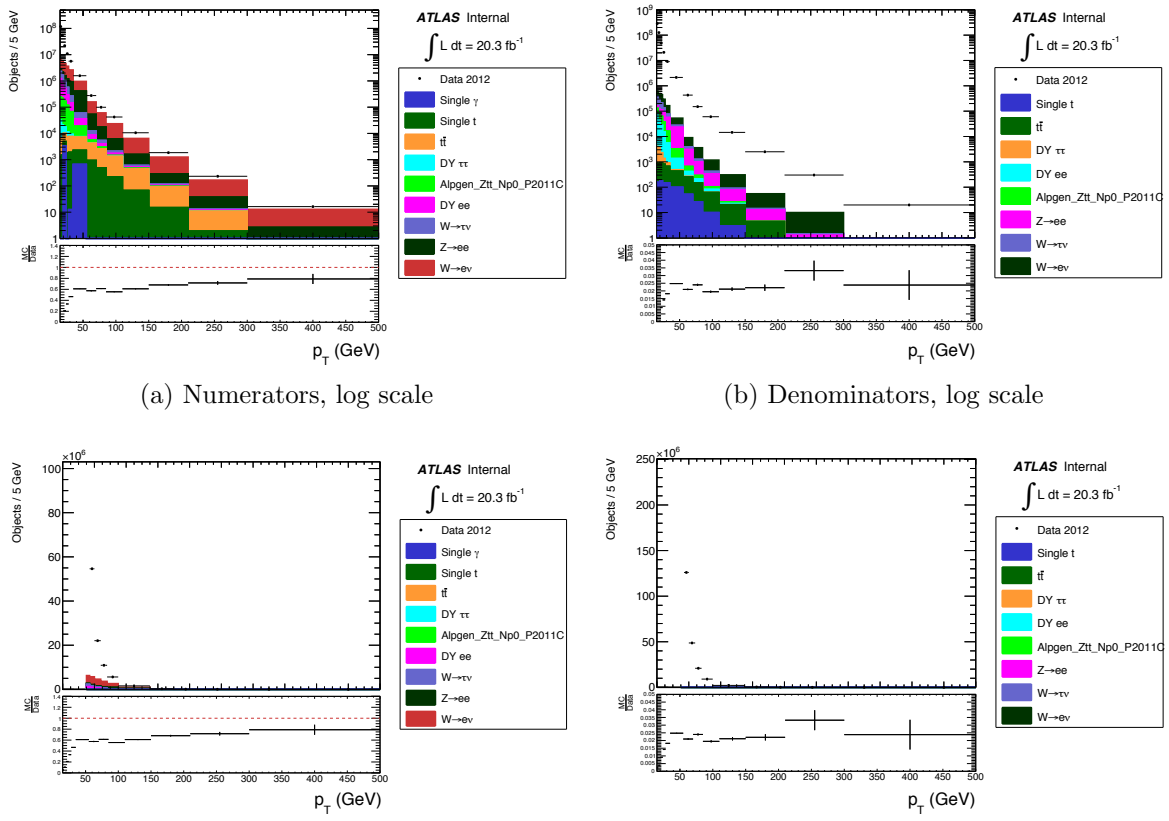

(a) Numerators, log scale

(b) Denominators, log scale

(c) Numerators, linear scale

(d) Denominators, linear scale

Figure 6.2: Numerator and denominator electron object counts. The data sample consists of all single-electron events in the 2012 dataset, with cuts to reduce prompt contamination as described in the text. The markers represent object counts from 2012 data, and the colored histograms indicate the prompt subtractions estimated from Monte Carlo.

whether a numerator or a denominator, in order to suppress prompt contamination from $Z \to ll$ events. The electrons are required to be trigger-matched to the trigger used to collect the event in the relevant p_{T} range. The residual prompt contamination, comprised mostly of W and Z events with smaller contributions from Drell-Yan, $t\bar{t}$ and single-t, is subtracted using Monte Carlo. The numerator and denominator event yields, as well as the predicted prompt contamination, are shown in figure 6.2. The prompt contamination consists primarily of W and Z events. The relative size of the prompt contamination is quite large for numerator objects, reaching up to $\sim 60\%$ for $p_{\mathrm{T}} \sim 50\,\mathrm{GeV}$, despite the cuts intended to reduce the W contribution. The fake factors are binned two-dimensionally in p_{T} and η, shown in figure 6.3. The p_{T} dependence of the fake factors is shown in figure 6.4, for the inclusive sample (left) and for various $|\eta|$ ranges (right).

To help clarify the origin of the structure in η observed at low p_{T}, the numerator and

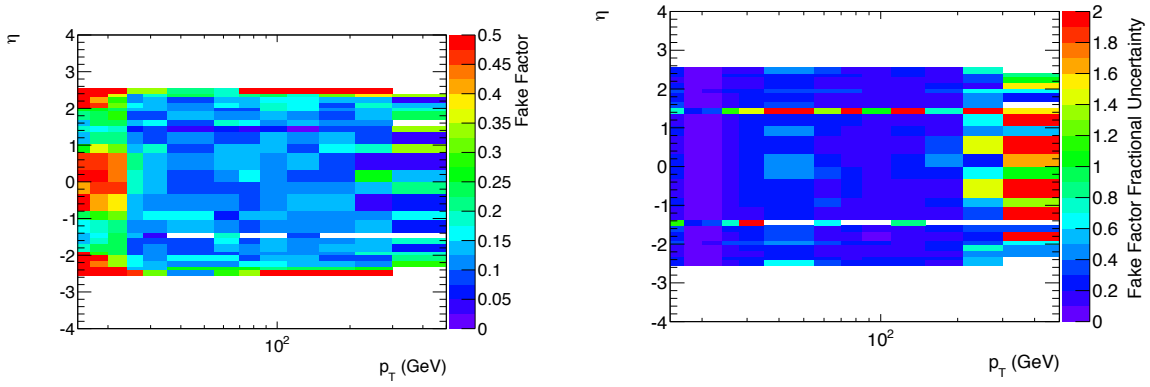

(a) Central values (b) Statistical uncertainty over value

Figure 6.3: Electron fake factors parametrized in p_T and η.

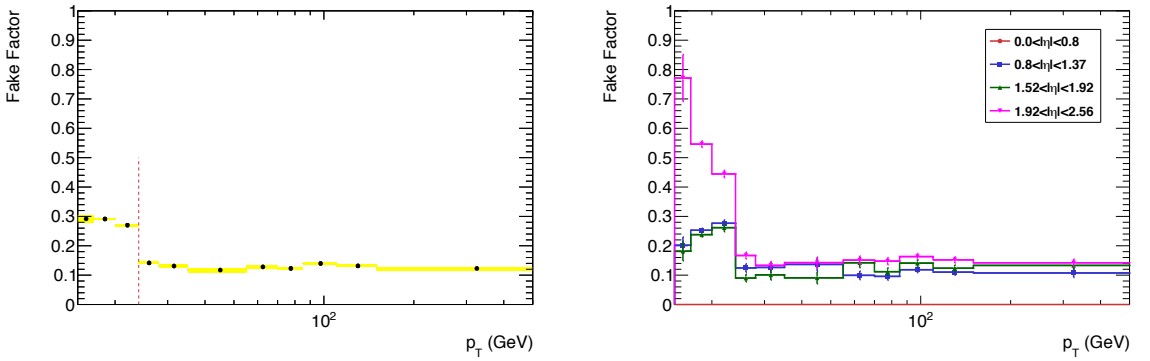

(a) Average fake factor vs. p_{T} (b) Fake factors vs. p_{T} for different value of electron $|\eta|$

Figure 6.4: Electron fake factors projected in p_{T}. The denominator requirements are different below and above 24 GeV, where the triggers switch from electron triggers to photon triggers; below, the additional requirements on $\Delta\eta_1$ and $\Delta\phi_2$ cause a large drop in the denominators, and a large increase in the fake factor values.

denominator counts are also shown versus η for $p_{\mathrm{T}} < 24\,\mathrm{GeV}$ in figure 6.5. The numerator counts are relative flat versus η in the central region, and grow for $|\eta| \gtrsim 2$. Conversely, the denominators exhibit a significant increase near the barrel-endcap overlap region, and also for $|\eta| \gtrsim 2$.

The following sources of systematic uncertainty are considered:

- **Prompt subtraction**: The presence of real, prompt leptons from Standard Model processes in the sample used to measure the fake factors is accounted for using Monte Carlo simulation. Uncertainties on the simulated samples include luminosity; cross

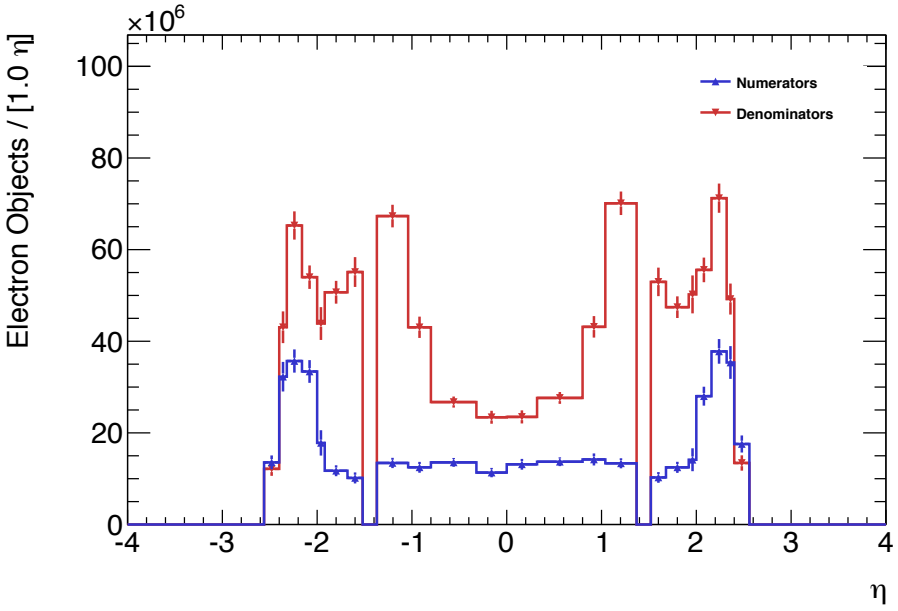

Figure 6.5: Electron numerator and denominator object counts versus η for $p_{\mathrm{T}} < 24\,\mathrm{GeV}$.

section uncertainties; and reconstruction, trigger, and identification efficiency scale factors. These lead to a maximum uncertainty of about 20% where the prompt subtraction is largest.

- **Trigger efficiency correction**: As mentioned previously, an inefficiency is observed in the loose electron triggers for offline `loose++` electrons. This is due to the lack of GSF tracking in the trigger. For the fake factor derivation, this affects electrons in the range $15\,\mathrm{GeV} < p_{\mathrm{T}} < 24\,\mathrm{GeV}$, where photon triggers are not available. Imposing the `tight++` cut on the track-cluster matching (the $\Delta\eta$ and $\Delta\phi$ between the electron track and calorimeter cluster) mitigates most, but not all, of the inefficiency, by cutting out electrons with large amounts of bremsstrahlung whose track are not reconstructed in the trigger. Based on a comparison of loose electron and photon triggers in the range $24\,\mathrm{GeV} < p_{\mathrm{T}} < 85\,\mathrm{GeV}$, a correction of about 8% is applied to loose electron-triggered events, and the same value is taken as systematic uncertainty.

- **Extrapolation to signal region**: Two systematic uncertainties are assigned to account for bias due to the extrapolation of fake factors from the control region to the signal region. First, the cuts on m_{T} and $E_{\mathrm{T}}^{\mathrm{miss}}$ are varied from $< 40\,\mathrm{GeV}$ to $< 25\,\mathrm{GeV}$ and $< 55\,\mathrm{GeV}$. A p_{T}-dependent systematic uncertainty of up to 15% is assigned. Second, Monte Carlo-based truth studies indicate that the fake factor values are quite different for heavy- and light-flavor jets, so a difference in heavy flavor fraction between the control and signal regions will bias the fake factors. The effect of this is estimated using a $t\bar{t}$ Monte Carlo sample, and a flat systematic uncertainty of 20% is assigned.

This study is described in section 10.1.1.

The systematic and combined statistical and systematic uncertainties on the fake factors are shown as a function of p_{T} in figure 6.6.

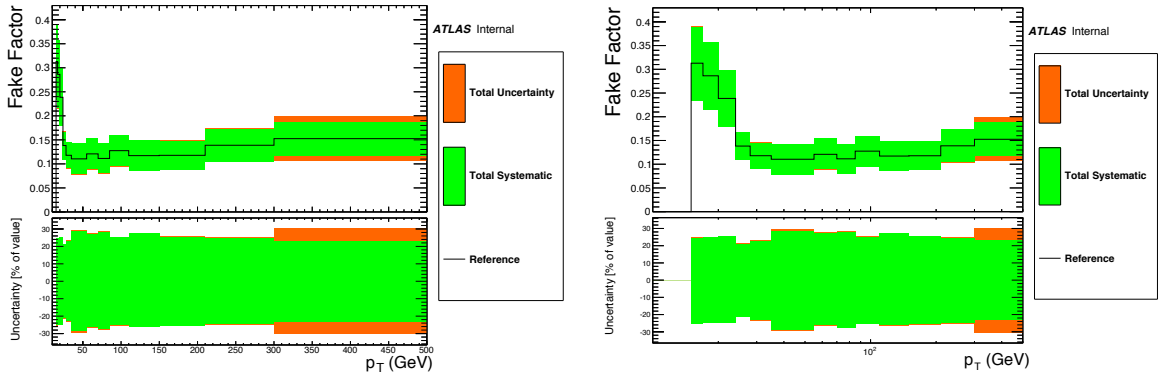

(a) Linear scale (b) Log scale

Figure 6.6: Electron fake factors vs. p_{T}, with systematic and combined statistical and systematic uncertainties. The statistical uncertainty includes both the data and prompt subtraction Monte Carlo statistics.

6.2.3 Muon Fake Factors

The muon fake factor method is similar to that used in the ATLAS same-sign dilepton search on the 7 TeV dataset [10]. The method targets non-prompt muons from semileptonic heavy flavor decays, punch-through, and decays-in-flight of long-lived mesons by inverting the isolation requirements. Specifically, the denominator muons are defined as follows:

- Pass all numerator muon requirements in table 5.2, except the requirements on `Etcone30`, `ptcone30`, and $\frac{d_0}{\sigma_{d_0}}$.
- Pass a looser impact parameter cut:

$$|\frac{d_0}{\sigma_{d_0}}| < 10 \tag{6.13}$$

- Invert isolation:

$$\texttt{Etcone30},\ \texttt{ptcone30} > \begin{cases} 0.15 p_{\mathrm{T}} & : \quad p_{\mathrm{T}} < 100\,\mathrm{GeV} \\ 15 + 0.01 p_{\mathrm{T}}\ \mathrm{GeV} & : \quad p_{\mathrm{T}} > 100\,\mathrm{GeV} \end{cases} \tag{6.14}$$

$$\frac{\texttt{Etcone30}}{p_{\mathrm{T}}} < 2.0 \tag{6.15}$$

$$\frac{\texttt{ptcone30}}{p_{\mathrm{T}}} < 2.0 \tag{6.16}$$

$$\tag{6.17}$$

- If $p_{\mathrm{T}} < 40\,\mathrm{GeV}$, apply the same overlap requirement as the signal regions, removing the muon if $\Delta R(\mu,\ \mathrm{jet}) < 0.3$. This overlap requirement is not applied for muons with $p_{\mathrm{T}} > 40\,\mathrm{GeV}$, which increases the statistical precision at the expense of additional systematic uncertainty. This is denoted by "dR" or "non-dR" below, for example in figure 6.9.

The muon fake factors are measured in a same-sign dimuon sample. The trigger used to collect the events requires two muons with $p_{\mathrm{T}} > 13\,\mathrm{GeV}$. The use of same-sign muons suppresses the prompt contamination from Z/γ^* events. The measurement uses only muons with large track impact parameter significance, $|\frac{d_0}{\sigma_{d_0}}| > 3$, to obtain a sample enriched in non-prompt muons (if both muons satisfy this requirement, then both are counted in the measurement). An extrapolation factor is derived from Monte Carlo to account for the fact that the signal region requires $|\frac{d_0}{\sigma_{d_0}}| < 3$, as detailed below.

Two sets of fake factors are measured, depending on the jet activity in the event. In the following, jets are required to have $p_{\mathrm{T}} > 30\,\mathrm{GeV}$, and be separated from muons with $\Delta R(\mu,\ \mathrm{jet}) > 0.3$.

- **Inclusive**: Applied to events with zero jets. The measurement uses the entire same-sign dimuon sample.

- **Two-Jet**: Applied to events with one or more jet. The measurement uses same-sign dimuon events with at least two jets with $p_{\mathrm{T}} > 30\,\mathrm{GeV}$.

Fake muons from the two-jet sample are expected to come primarily from W + jets and $t\bar{t}$ processes, while the inclusive sample also includes contributions from $b\bar{b}$. Figure 6.7 shows the p_{T} distributions of numerator and denominator muons in the measurement sample along with the expected prompt contributions.

The extrapolation factor from the measurement control region, with $|\frac{d_0}{\sigma_{d_0}}| > 3$, to the signal region, with $|\frac{d_0}{\sigma_{d_0}}| < 3$, is derived from various Monte Carlo samples. The extrapolation factor is simply the ratio of fake factors derived in Monte Carlo using the control region cut ($|\frac{d_0}{\sigma_{d_0}}| > 3$) to those using the signal region cut ($|\frac{d_0}{\sigma_{d_0}}| < 3$). The central value is taken from the POWHEG $t\bar{t}$ sample, using all truth-level non-prompt muons, as shown in figure 6.8.

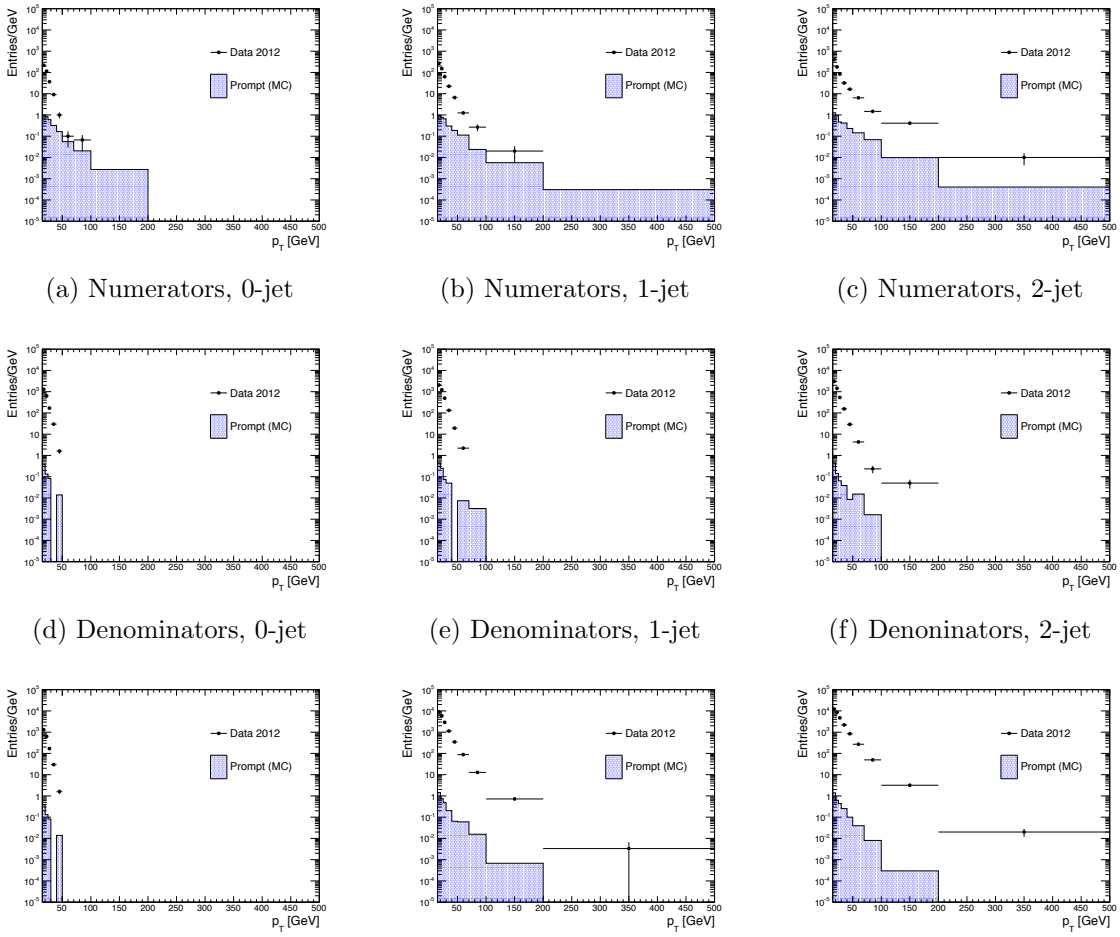

(a) Numerators, 0-jet (b) Numerators, 1-jet (c) Numerators, 2-jet

(d) Denominators, 0-jet (e) Denominators, 1-jet (f) Denoninators, 2-jet

(g) Denominators, 0-jet (h) Denominators, 1-jet (i) Denominators, 2-jet

Figure 6.7: p_{T} spectrum of muons used in fake factor measurement. The left plots show events with zero jets, the middle plots show events with one jet, and the right plots show events with two or more jets. All numerator events require both numerator and denominator be separated from a jet by $\Delta R > 0.3$; the same requirement is applied to denominators in the second row of plots, while the third row shows denominators that are not required to be isolated from nearby jets.

A systematic uncertainty is assigned by comparing with other samples (MC@NLO $t\bar{t}$ and PYTHIAB $b\bar{b}$ and $c\bar{c}$), and using only same-sign dimuon events in these samples.

The fake factors are parametrized one-dimensionally in p_{T} and η, as there are insufficient statistics to do a full two-dimensional parametrization. The fake factor is computed as:

$$f(p_{\mathrm{T}},\ \eta) = \frac{f(p_{\mathrm{T}}) \times f(\eta)}{\langle f \rangle} \tag{6.18}$$

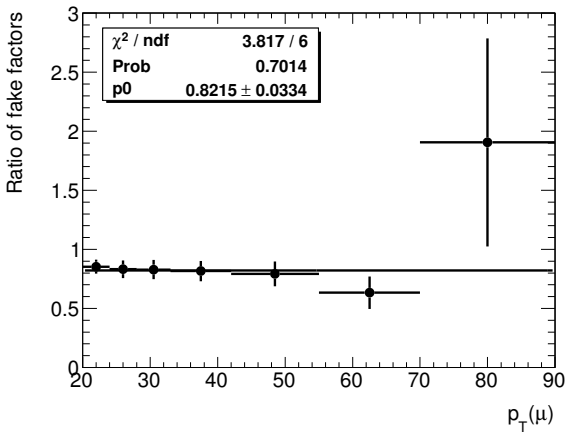

Figure 6.8: Ratio between the fake factors for muons with $|d_0|/\sigma(d_0) > 3$ compared to fake factors with nominal numerator and denominator definitions. These fake factors are derived from a POWHEG $t\bar{t}$ sample.

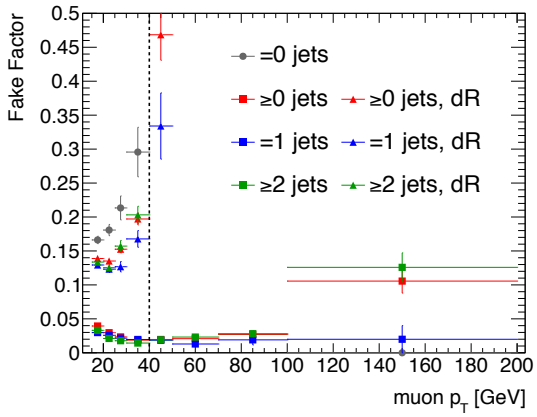

Figure 6.9: Muon fake factors as a function of p_{T}. Two sets of fake factors are plotted, with and without the "dR" requirement. The vertical dashed line at 40 GeV indicates the point at which the fake factors switch from the "dR" points, where the denominators are required to be separated from nearby jets, to the lower, non-"dR" points where the jet-isolation requirement is dropped to improve the statistics.

where $\langle f \rangle$ is the total average fake factor. The measured fake factors are shown in figures 6.9 and 6.10.

The sources of systematic uncertainty considered are listed below, and the fractional systematic uncertainty is shown in figure 6.11.

- **Prompt subtraction**: The normalization of the simulated prompt subtraction samples is varied by ±10%, leading to a systematic uncertainty of 1%–6%.

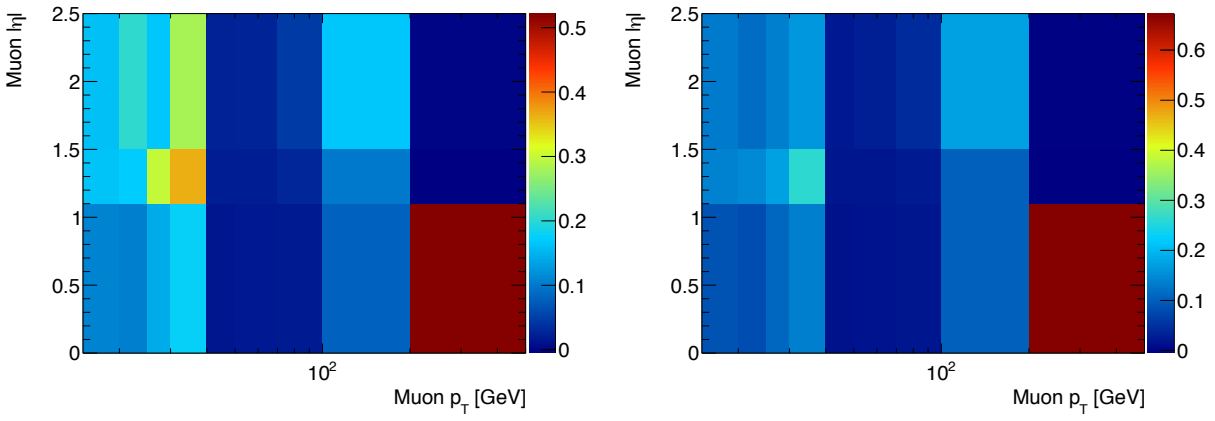

(a) Inclusive FF (b) Two-jet FF

Figure 6.10: Muon fake factors as functions of p_{T} and $|\eta|$. The left plot shows fake factors measured in the inclusive control sample and applied to events with zero jets. The right plot shows fake factors measured in events with two jets, and applied to events with at least one jet.

- **Topological dependence**: The difference between the inclusive and two-jet fake factors is taken as a systematic uncertainty. The uncertainty is symmetrized, using the full difference as both upward and downward uncertainty, and ranges from 3% to 36%.
- **Dependence on d_0 significance**: As mentioned previously, the extrapolation factor is derived in a number of different Monte Carlo samples. The largest deviation of 24% is taken as a systematic uncertainty.
- **Light flavor fraction**: As with the electron fake factors, the fake factor values are quite different for muons originating from light flavor (LF) sources (π/K decay or punch-through) versus heavy flavor (HF) decays. The systematic uncertainty is derived using the difference in momenta measured by the inner detector and muon spectrometer as a discriminant between HF and LF fakes. The difference in HF/LF fraction between the control and signal regions is estimated, and the HF and LF fake factors measured in Monte Carlo are used to estimate the effect of the discrepancy in HF/LF fraction. A systematic uncertainty of 2% to 21% is assigned.

6.2.4 Tau Lepton Fakes

The detector signature of hadronically decaying tau leptons, consisting of a jet with one or more associated tracks, is not as distinctive as the signature of electrons and muons. Differentiating between jets, which are copiously produced in proton-proton collisions, and

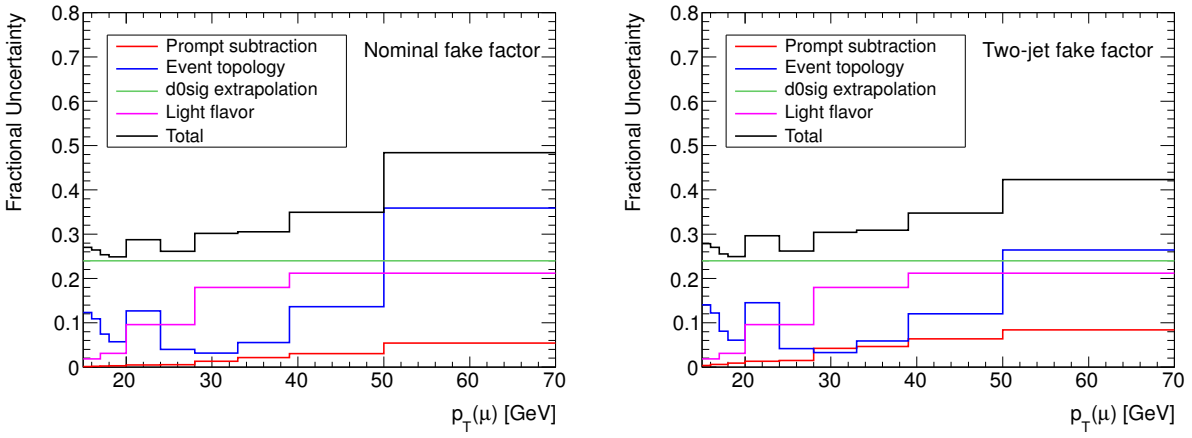

(a) Inclusive FF (b) Two-jet FF

Figure 6.11: Systematic uncertainties on muon fake factor as a function of $p_{\mathrm{T}}(\mu)$. The left plot shows the uncertainties for the inclusive fake factor, while the right shows the uncertainty for the two-jet fake factor.

hadronically decaying tau leptons is difficult, and accordingly the reducible backgrounds in events containing a hadronically decaying tau lepton is much larger.

The tau identification algorithm (section 5.4) employs a multivariate discriminant based on calorimeter shower shapes and tracking information. The fake rate is strongly dependent on the jet fragmentation, in particular whether the parton initiating the jet is a gluon, light quark, or heavy quark. In constructing the denominator definition, a tighter efficiency working point reduces the dependence on the initial parton, thereby improving the extrapolation of the fake factors to the signal regions; on the other hand, the working point must be loose enough to collect sufficient statistics. The denominator definition requires tau candidates to have a `BDTScore` which fails the `BDT-Medium` selection threshold, but exceeds 0.9 times the p_{T}-dependent `BDT-Loose` threshold. In simulation, this definition is seen to be relatively insensitive to the type of parton initiating the jet. The fake factors are measured two-dimensionally in bins of p_{T} and $|\eta|$, and a correction is applied as a function of the highest MV1 b-tag weight of all jets in the event.

Fake Factor Measurement

The tau lepton fake factors are measured using a tag-and-probe method in a sample targeting W+jets events. Events are required to have a muon satisfying the numerator criteria (tag) plus a hadronic tau candidate (probe). To avoid biasing the fake factors, no other requirements are imposed to reject the prompt contamination (for example, requiring the muon and $\tau_{\text{had-vis}}$ to have the same sign biases the sample towards gluon-initiated jets). The prompt contamination, dominantly from Z+jets and $t\bar{t}$ production, is subtracted using simulation.

The muon-$\tau_{\text{had-vis}}$ invariant mass and $\tau_{\text{had-vis}}$ p_{T} spectra for numerators and denominators are shown in figure 6.12, along with the prompt contribution estimated from simulation. Figure 6.13 shows the resulting fake factors.

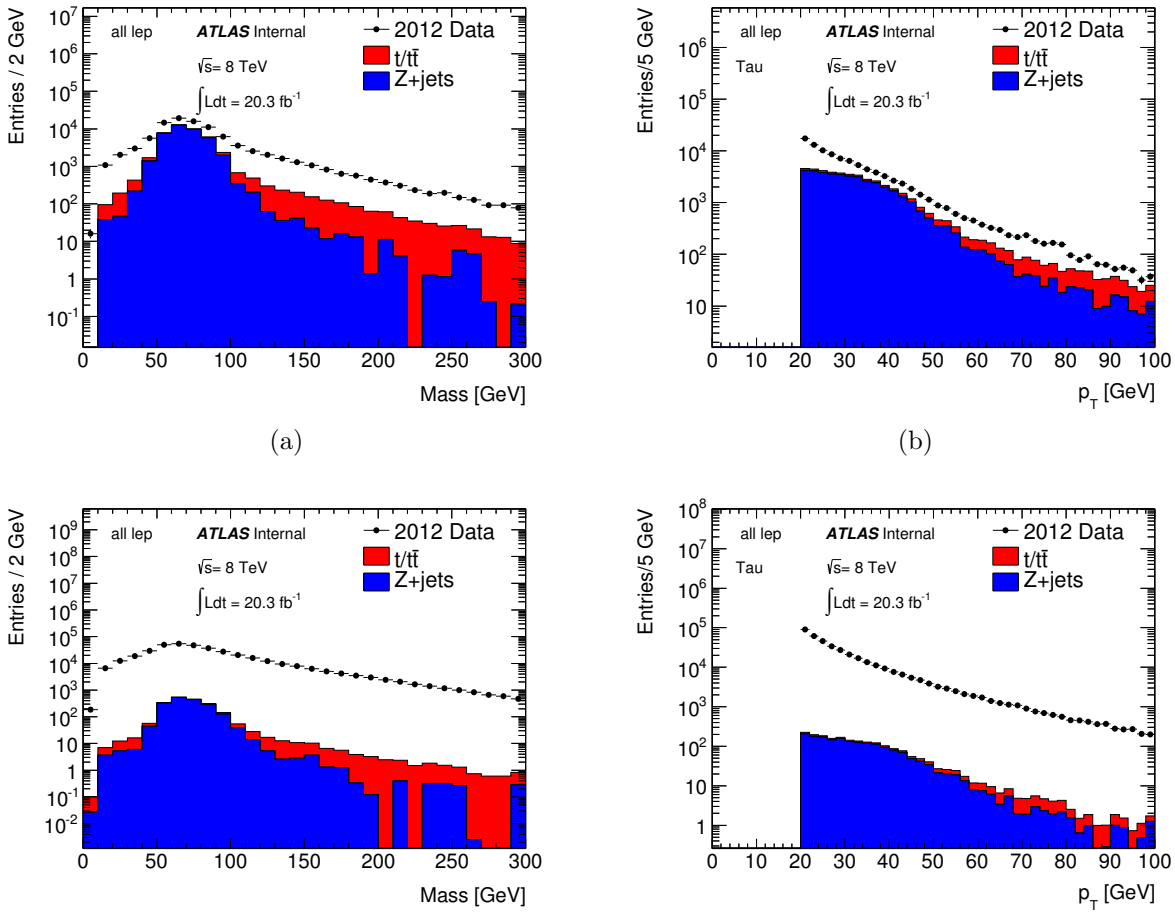

Figure 6.12: Invariant mass of the muon and $\tau_{\text{had-vis}}$ pair (left) and p_{T} of the tau candidate (right). The top plots show the distributions for numerator $\tau_{\text{had-vis}}$ candidates, while the bottom plots show the distributions for denominator $\tau_{\text{had-vis}}$ candidates. The filled histograms show the prompt contamination estimated from simulation.

Systematic Uncertainties

The following sources of systematics uncertainties on the tau fake factors are considered:

- Uncertainties on the simulation-based estimates of the prompt contamination.

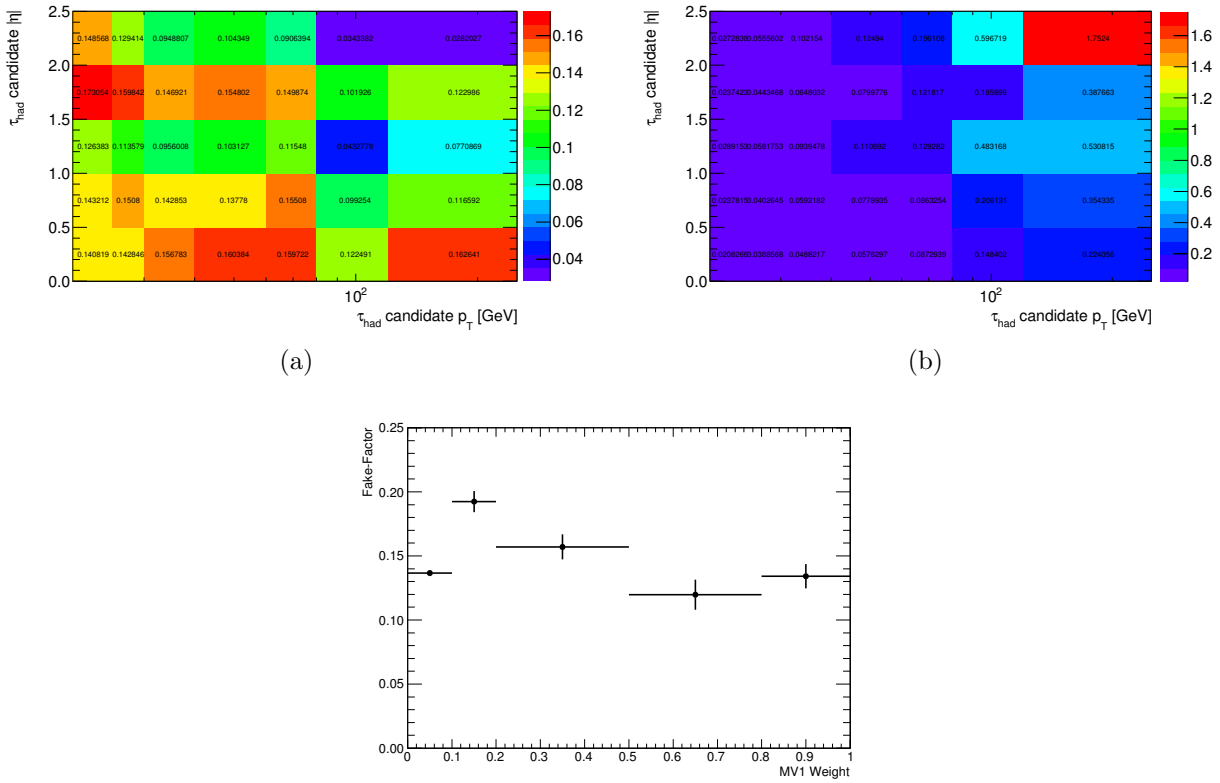

Figure 6.13: Tau fake factors binned in p_{T} and $|\eta|$ (left), and the corresponding statistical uncertainty (right). The correction for the maximum MV1 b-tag weight of all jets in the event is also shown (bottom). The fake factors are derived from W+jets events.

- Uncertainties associated with the binning choice.
- Dependence of the fake factors on the flavor of the initiating parton.

The uncertainty due to the prompt contamination estimatation is derived by fluctuating the normalizations of the Monte Carlo samples by their theoretical uncertainties. The resulting variations in the fake factors are between 5%-17%, and are largest for $30\,\mathrm{GeV} \lesssim p_{\mathrm{T}} \lesssim 40\,\mathrm{GeV}$, where the contribution from $Z \to \tau_\mu \tau_{\mathrm{had}}$ is greatest.

To estimate the effect of the binning, the fake factors are reapplied to the same sample they were derived from. The results are shown in figure 6.14. An uncertainty of 5% is assigned.

Finally, to estimate the effect of differences in flavor composition between the measurement sample and the signal regions, the fake factors are applied to a $t\bar{t}$ validation region. In simulation, this validation region is observed to have a substantially different flavor compo-

sition from the W+jets measurement sample. A systematic uncertainty of 25% covers the observed differences between the fake background estimate and the data.

In total, the systematic uncertainties are in the range 25%-30%, and are largest around $30\,\text{GeV} \lesssim p_{\text{T}} \lesssim 40\,\text{GeV}$.

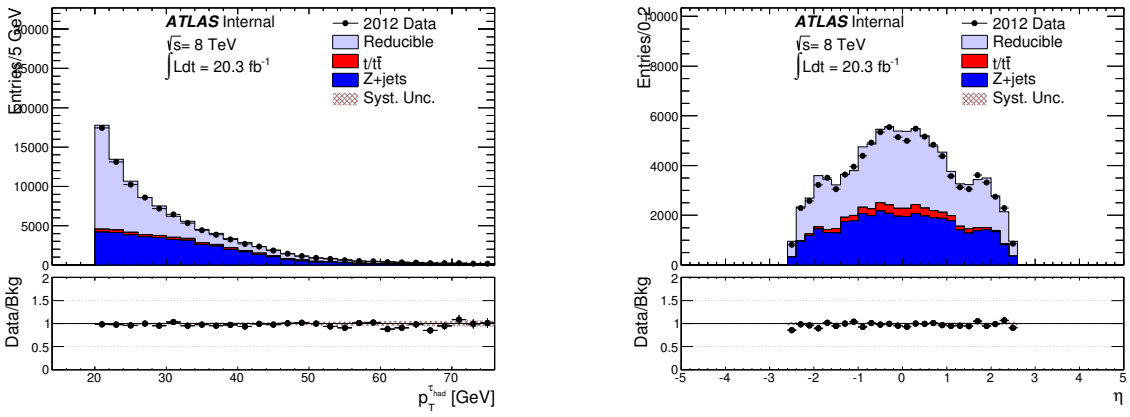

(a) (b)

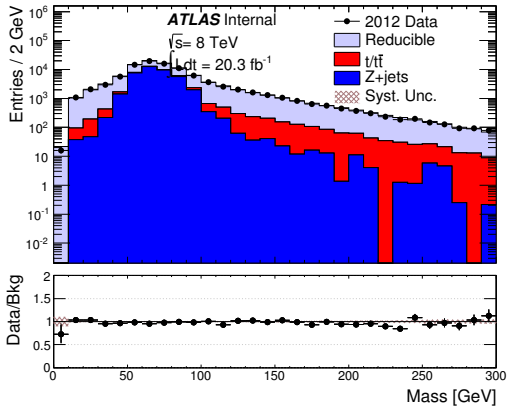

(c)

Figure 6.14: Results of the closure test, comparing the data to the fake factor-based background estimate in a $t\bar{t}$ validation region. The $\tau_{\text{had-vis}}$ p_{T} (left), $|\eta|$ (right), and the dilepton invariant mass (bottom) are shown.